

Characterization of viscoelastic media using reverberant shear wave autocorrelation estimator

Sedigheh S. Poul^{1,†}, Juvenal Ormachea², Kevin J. Parker³

¹Department of Mechanical Engineering, University of Rochester, Rochester, NY, USA, 14627.

²Verasonics Inc., Kirkland, WA, USA, 98034.

³Department of Electrical and Computer Engineering, University of Rochester, Rochester, NY, USA, 14627.

ABSTRACT

The reverberant shear wave (RSW) technique offers a promising framework for elastography. In this study, to characterize fibrotic fatty livers at different fibrotic stages, we employed an autocorrelation (AC) estimator within the RSW framework to evaluate shear wave speed (SWS) of viscoelastic media. To this end, we utilized both simulation and experimental approaches and excited the RSW field in a medium within each approach at the frequency of 150 Hz: (i) the finite element (FE) simulation of a RSW field in a 3D model of a whole organ fatty liver and (ii) the RSW experiments on two castor-oil-in-gelatin phantoms fabricated in the lab. In the FE simulations, to represent a more realistic liver model, a thin adipose fat layer and a muscle layer were added as viscoelastic power-law materials on top of the liver model. The SWS estimation from the RSW simulation was compared with predictions from the theory of composite media for verification. For the RSW experiments on phantoms, the SWS estimations were compared with the SWS results obtained from performing the stress relaxation test as an independent modality. The simulation results showed that the RSW-based AC estimator provides good estimates of SWS, within >90% accuracy compared with theory. Also, the RSW estimator results from the phantom experiments at different background stiffness levels provided some experimental support for the utility of the RSW estimator. These results demonstrated that the AC estimator is sensitive to the changes in viscoelastic properties of viscoelastic media.

Keywords: Elastography, reverberant shear wave, shear wave speed, autocorrelation estimator, finite element modeling.

1. INTRODUCTION

Elastography aims at characterizing pathological changes of tissues by measuring tissues' biomechanical properties. Shear wave (SW) based elastography relies on measuring the response of a tissue to shear wave excitations to derive mechanical properties of the underlying tissue^{1,2}. Different SW based approaches have been employed to measure the viscoelastic properties such as shear wave speed (SWS), shear wave attenuation and shear wave dispersion in soft tissues or tissue-mimicking media³⁻¹². Recently, the reverberant shear wave (RSW) approach has been proposed by Parker et al.¹³ as a novel elastography technique for imaging the SWS by exciting a random 3D distribution of harmonic shear waves. One advantage of the RSW approach is that it does not require directional filtering to eliminate reflections from boundaries, and further, it benefits from all reflections as secondary sources producing a better and more random reverberation field. This technique provides two different estimators for characterizing SWS: (i) the autocorrelation (AC) estimator and (ii) the phase gradient estimator^{14,15}. In this study, we employ the AC estimator to characterize viscoelastic media in a 3D model of fatty liver using simulations as well as tissue-mimicking phantoms to evaluate the sensitivity of this estimator to the changes in the fibrosis (stiffness) levels. We then compare the results with some independent measurements for verification.

[†] Corresponding author, (Sedigheh S. Poul, Email: poul@rochester.edu)

2. THEORY

In a fully developed RSW field within a domain, estimating the wavenumber k is the main goal of assessing the AC estimator since the wavenumber is related to SWS (c_s) through frequency f as shown in equation (1). In a RSW field, if $v_z(x, z)$ represents the complex axial velocity field in a 2D plane within the domain and k_x and k_z denote the lateral and axial wavenumbers, respectively, the lateral AC and axial AC of the velocity field as a function of their associated wavenumbers are obtained from equations (2) and (3), respectively. Having the particle displacement field within a medium, one can calculate the lateral and axial ACs of the data and fit them to these equations to obtain k_x and k_z (and therefore, the average wavenumber). In these equations, j_0 and j_1 are the first kind spherical Bessel functions of zero order and first order, respectively. $\Delta\varepsilon_x$ and $\Delta\varepsilon_z$ are spatial lags and β_x and β_z are some constants.

$$c_s = \frac{2\pi f}{k} \quad (1)$$

$$B_{v_z v_z}(\Delta\varepsilon_x) = \frac{\beta_x}{2} \left[j_0(k_x \Delta\varepsilon_x) - \frac{j_1(k_x \Delta\varepsilon_x)}{k_x \Delta\varepsilon_x} \right] \quad (2)$$

$$B_{v_z v_z}(\Delta\varepsilon_z) = \frac{\beta_z}{2} \left[\frac{j_1(k_z \Delta\varepsilon_z)}{k_z \Delta\varepsilon_z} \right] \quad (3)$$

An independent theoretical approach for predicting the SWS in a fatty liver is the theory of composite media¹⁶. Assuming the shear moduli of the background medium and fat inclusions to be $G_1(\omega)$ and $G_2(\omega)$, respectively and the fat volume fraction distributed within the medium is denoted by V_2 , the shear modulus of the composite fatty media $G_c(\omega)$ as a function of angular frequency ω is obtained from equation (4). The complex modulus is employed to obtain SWS according to equation (5) in which ρ is the density of the medium.

$$G_c(\omega) = G_1(\omega) \cdot \left\{ 1 - \frac{5[G_1(\omega) - G_2(\omega)]V_2}{3G_1(\omega) + 2G_2(\omega)} \right\} = G_{storage}(\omega) + jG_{loss}(\omega) \quad (4)$$

$$c_s(\omega) = |G_c(\omega)| \sqrt{\frac{2}{\rho(|G_c(\omega)| + G_{storage}(\omega))}} \quad (5)$$

3. METHODS

1.1. Finite element simulation of RSW field

For the simulation studies, a 3D model of a liver encompassed by a thin layer of adipose fat material on top and an outer layer of muscle material was considered to represent a more realistic model of liver in RSW experiments. The 3D liver geometry is shown in **Figure 1 (a)**. The RSW field within the 3D liver model was simulated by a finite element (FE) analysis approach using Abaqus/CAE 2019 software (Dassault Systems, Vélizy-Villacoublay Cedex, France) using the direct steady state dynamic method. The excitation forces were applied as dipole pairs of upward-downward normal traction forces on the muscle layer. Two different stiffness levels (based on METAVIR fibrosis stages F0 and F3¹⁷) with fat inclusions of 24% were modeled at the excitation frequency of 150 Hz. The liver tissue, fat layer, and muscle layer were modeled as power-law viscoelastic materials with the power-law parameters of 0.12, 0.04, and 0.03, respectively, consistent with the values reported in the literature. The fat inclusions material distributed in the liver is also modeled as a frequency-dependent material set to behave as a nearly pure viscous material. The number of elements used to mesh the 3D model was 1,200,000. The fat inclusions were randomly distributed within the 3D liver model at 24% volume fraction of the liver. The exported outputs from Abaqus simulations were the complex axial velocity field, along the z direction (v_z), and the spatial coordinates.

1.2. RSW experiment on phantom

For the experimental study, two viscoelastic oil-in-gelatin phantoms were fabricated in the lab at two different gelatin concentrations of 5% and 7%, each having 12% castor oil inclusions. The details of the phantom fabrication process is reported in^{16, 18}. The RSWs were generated within the phantoms using three custom-made vibrators and a mini-shaker (Type 4810, Brüel & Kjær, Virum, Denmark) as shown in **Figure 1 (b)**, all simultaneously vibrating at the frequency of

150 Hz. A Verasonics ultrasound system (Vantage-128™, Verasonics, Kirkland, WA, USA), was employed to track the particle displacement¹³.



Figure 1: (a) 3D model of liver (red color) surrounded by a layer of fat (cream color) and muscle (brown color) for FE simulations. (b) Experimental set-up for RSW experiment on a phantom with 7% gelatin and 12% castor oil.

For assessing the RSW experimental results after scanning each phantom, the stress relaxation (SR) test as an independent modality was performed on small cylindrical samples cut from each phantom with a maximum strain of was 7% [mm/mm]. The experimental SR data were fitted to the Kelvin-Voigt’s fractional derivative (KVFD) model to estimate the model parameters and then, evaluate SWS using the fitting results. The details of the SR tests and also the fitting process are fully explained in a recent study^{16, 19}.

4. RESULTS AND DISCUSSION

Figure 2 (a) and (b) show the RSW results from the simulation for F0 and F3 fibrosis cases, respectively. In this figure, (1) shows the simulated RSW fields generated in a 2D plane (x - z) within the 3D model, (2) is the 2D AC profile for the

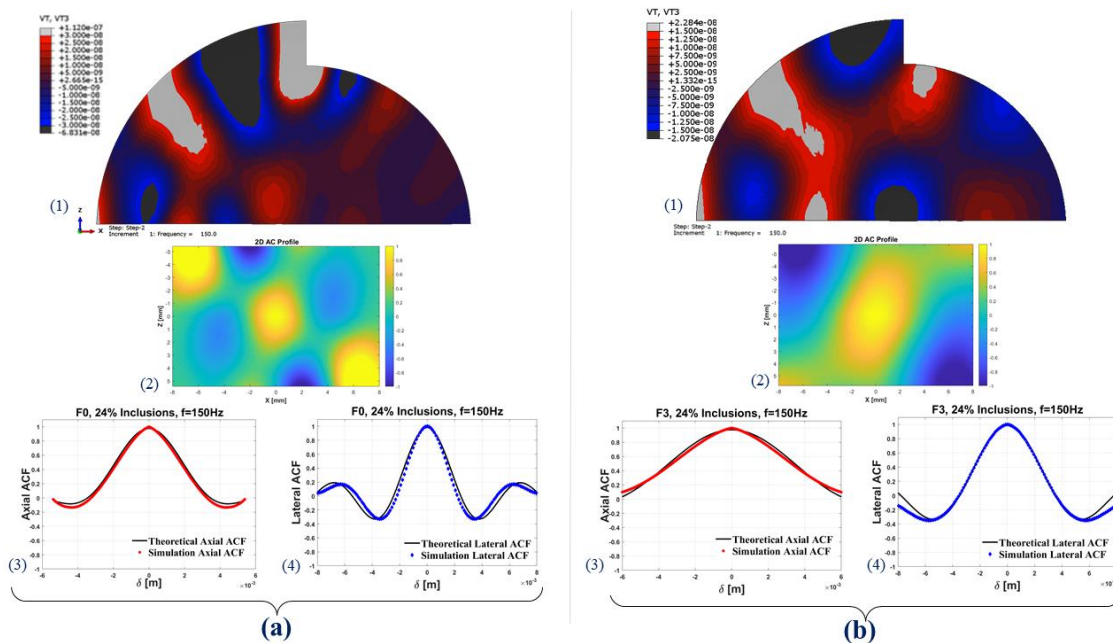


Figure 2: RSW simulation results for case with (a) F0 fibrosis and (b) F3 fibrosis, both with 24% fat inclusions. (1) shows the 2D (x - z) view of the particle velocity field on a plane within 3D liver model. (2) is the 2D AC profile calculated from a central region in (1). (3) and (4) are the axial and lateral AC profiles in simulation, respectively fitted to the theory.

complex particle velocity extracted from the center region of the 2D plane, (3) and (4) show axial and lateral AC profiles, respectively, fitted to the theory. It is noted that in the (x - z) plane cut from the 3D liver model shown in (1), the muscle and fat layers are located in the left side of the plane.

From this figure, it is observed that the RSW field is stronger close to the abdomen front where excitation forces are located and gets attenuated by traveling (to the right side) through the viscoelastic liver. The wavefronts in the left regions show some changes in transitioning from the muscle layer to the fat layer or from the fat layer to the liver region. Moreover, it is demonstrated that the wavefront is perturbed by the presence of fat inclusions. The simulated AC data are shown to be well-fitted to the theoretical AC profiles. Moreover, comparing the simulation results for the F0 and F3 fibrosis stages, it is observed that the wavelength of the RSW propagating wave as well as the AC profile width are smaller in the F0 case than in the F3 case which is consistent with the elevated SWS in the more advanced fibrosis stage, i.e., the F3 case.

Figure 3 (a) and (b) show experimental RSW tests on the viscoelastic phantoms having 7% and 5% gelatin, respectively at the frequency of 150 Hz. In this figure, (1) illustrates the RSW field produced within the phantoms on a 2D plane cut, (2) is the B-scan, and (3) shows the 2D SWS image obtained from AC estimator overlaid on the B-scan. Increasing gelatin concentration is expected to make the viscoelastic phantom stiffer. Comparing the two SWS images from the two phantoms, it is observed that AC estimator calculates higher SWS values for the phantom having the higher gelatin concentration (7%), which corresponds to an increased stiffness level. This indicates that the AC estimator is sensitive to the changes in the background stiffness within phantoms with castor oil inclusions.

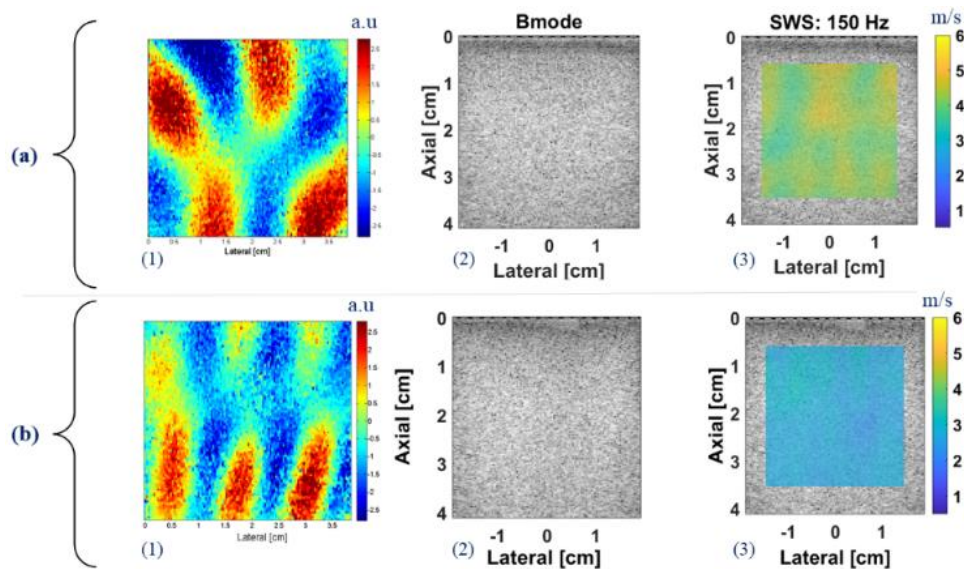


Figure 3: RSW experimental results on phantom with: (a) 7% gelatin and 12% castor oil, (b) 5% gelatin and 12% castor oil. (1) shows the RSW field generated within the phantom at the frequency of 150Hz, (2) is the B-scan, (3) demonstrates the SWS map obtained from the AC estimator at 150Hz overlaid on the B-scan.

For verification of the magnitude of SWS results obtained from the AC estimator in the last two sections, the SWS values in simulation cases and experiments on phantoms are compared with SWS predictions from the theory of composite media and the SWS from SR tests on phantoms, respectively. The SR results on phantoms fitted to the KVFD model are presented in **Figure 4**.

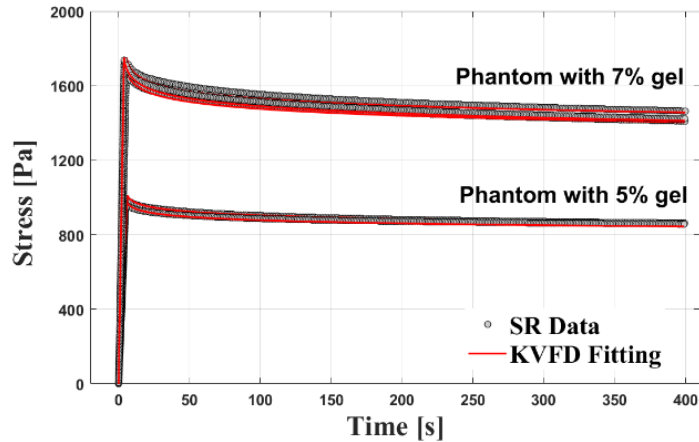


Figure 4: SR results on different samples from the two phantoms fitted to the KVFD model.

The two pairs of SWS comparisons are depicted in **Figure 5** for the verification of the simulation and experimental results. As a telling observation, there are reasonable agreements in each pair, indicating the accurate predictions from applying the AC estimator within the RSW framework. This agreement in the phantom test is less pronounced which may result from the small size of the samples for the SR test not representing the whole phantom and also pre-straining due to the applied force of the transducer resting on the surface of the phantom during the RSW scans. These observations will be studied in the future work with more extensive phantom studies.

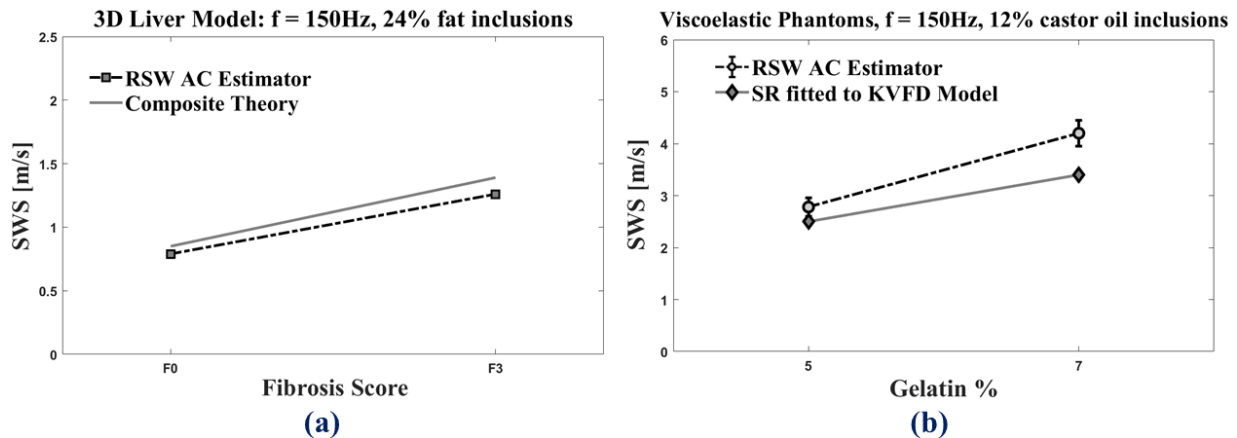


Figure 5: (a) Comparison of SWS from RSW simulations with the theory of composite theory. (b) Comparison of SWS from RSW experiments on phantoms with the SWS from SR tests on phantoms as an independent test.

5. CONCLUSION

In this study, we showed that the RSW-based AC estimator is sensitive to variation in fibrosis stage (stiffness). It provides a good estimation of SWS within the 3D model of fatty liver compared with the theory of composite media, with >90% accuracy and a close estimation of SWS in viscoelastic phantoms compared with the SR test as an independent modality. However, it is noted that this agreement is partially weaker in oil-in-gelatin phantom experiments. Overall, the RSW-based estimator works reasonably well in estimating the SWS in viscoelastic media.

ACKNOWLEDGMENT

This work was supported by National Institutes of Health grants R21EB025290 and R21AG070331.

REFERENCES

- [1] J. Ormachea, and K. J. Parker, "Elastography imaging: the 30 year perspective," *Physics in Medicine & Biology* **65**(24), 24TR06 (2020).
- [2] H. Li et al., "Viscoelasticity imaging of biological tissues and single cells using shear wave propagation," *Viscoelasticity: From Individual Cell Behavior to Collective Tissue Remodeling* (2021).
- [3] I. Z. Nenadic et al., "Attenuation measuring ultrasound shearwave elastography and in vivo application in post-transplant liver patients," *Physics in Medicine & Biology* **62**(2), 484 (2016).
- [4] V. Kumar et al., "Viscoelastic parameters as discriminators of breast masses: Initial human study results," *PloS one* **13**(10), e0205717 (2018).
- [5] K. R. Nightingale et al., "Derivation and analysis of viscoelastic properties in human liver: impact of frequency on fibrosis and steatosis staging," *IEEE transactions on ultrasonics, ferroelectrics, and frequency control* **62**(1), 165-175 (2015).
- [6] S. Chen, M. Fatemi, and J. F. Greenleaf, "Quantifying elasticity and viscosity from measurement of shear wave speed dispersion," *The Journal of the Acoustical Society of America* **115**(6), 2781-2785 (2004).
- [7] S. Bernard, S. Kazemirad, and G. Cloutier, "A frequency-shift method to measure shear-wave attenuation in soft tissues," *IEEE transactions on ultrasonics, ferroelectrics, and frequency control* **64**(3), 514-524 (2016).
- [8] M. Tanter et al., "Quantitative assessment of breast lesion viscoelasticity: initial clinical results using supersonic shear imaging," *Ultrasound in medicine & biology* **34**(9), 1373-1386 (2008).
- [9] K. J. Parker et al., "Analysis of transient shear wave in lossy media," *Ultrasound in medicine & biology* **44**(7), 1504-1515 (2018).
- [10] S. Catheline et al., "Measurement of viscoelastic properties of homogeneous soft solid using transient elastography: An inverse problem approach," *The Journal of the Acoustical Society of America* **116**(6), 3734-3741 (2004).
- [11] A. Nabavizadeh et al., "Viscoelastic biomarker for differentiation of benign and malignant breast lesion in ultra-low frequency range," *Scientific reports* **9**(1), 1-12 (2019).
- [12] M. L. Palmeri et al., "Quantifying hepatic shear modulus in vivo using acoustic radiation force," *Ultrasound in medicine & biology* **34**(4), 546-558 (2008).
- [13] K. J. Parker et al., "Reverberant shear wave fields and estimation of tissue properties," *Physics in Medicine & Biology* **62**(3), 1046 (2017).
- [14] F. Zvietcovich et al., "Reverberant 3D optical coherence elastography maps the elasticity of individual corneal layers," *Nature communications* **10**(1), 1-13 (2019).
- [15] J. Ormachea, and K. Parker, "Reverberant shear wave phase gradients for elastography," *Physics in Medicine & Biology* **66**(17), 175001 (2021).
- [16] S. S. Poul, and K. J. Parker, "Fat and fibrosis as confounding cofactors in viscoelastic measurements of the liver," *Physics in Medicine & Biology* **66**(4), 045024 (2021).
- [17] R. G. Barr et al., "Elastography assessment of liver fibrosis: society of radiologists in ultrasound consensus conference statement," *Radiology* **276**(3), 845-861 (2015).
- [18] S. S. Poul et al., "Validations of the microchannel flow model for characterizing vascularized tissues," *Fluids* **5**(4), 228 (2020).
- [19] S. Poul et al., "Comprehensive Experimental Assessments of Rheological Models' Performance in Elastography of Soft Tissues," *Available at SSRN 4036156*.